RESEARCH

Silk sericin-hydroxyapatite nanoribbons toward structurally stable osteogenic scaffolds

Nazan Goksen Tosun[1] · Ali Ozer[2,3] · Tugba Bektas[1] · Kerim Emre Oksuz[2] · Secil Erden Tayhan[4] · Tugba Ozdemir[5]

Abstract
Building a successful, cost-effective, and natural solution toward improving the bone-implant interface is an outstanding challenge. Silkworm sericin attracted the attention of bone researchers in the past decade due to its unexpected performance toward inherently promoting osteogenic differentiation of progenitor/stem cells. Hydroxyapatite is widely utilized in bone tissue regenerative scaffolds as the majority of bone matrix is constituted of inorganic material, primarily hydroxyapatite. Combining sericin and hydroxyapatite pledges improved mineralization performance in a bone regenerative scaffold which could increase the success of implanted bone biomaterial interfaces. Through electrospinning, we produced sericin and hydroxyapatite nanoribbons to present a high surface area and porous scaffold to culture osteoprogenitors and aimed to enhance cell adhesion and proliferation ultimately improving mineralization density. Material characterization is performed through field emission scanning electron microscopy, energy dispersive spectroscopy, and Fourier transform infrared spectroscopy. We showed that the addition of hydroxyapatite into sericin nanoribbons significantly enhanced cell proliferation and cytoskeletal organization in vitro and detected an overall improvement in mineral density. We propose that sericin nanoribbons reinforced with hydroxyapatite are suitable platforms for further bone regenerative interface applications.

Keywords Sericin · Hydroxyapatite · Osteoinduction · Bone · Implant

Introduction

The ideal interfacial scaffold between the bone tissue and the implant material should possess three characteristics [1]. First, it must be osteoconductive, to accommodate the space needed for newly forming bone tissue and vasculature. Second, it must be osteoinductive, to drive stem cell differentiation and expression of *osteogenic* differentiation proteins. Finally, it must be osteogenic to enhance mineralization and proper calcification of the newly formed tissue as well as osteogenic differentiation of progenitor cells. It is desirable for a bone tissue engineering material to show all three characteristics; however, due to both the organic and mineral-containing nature of bone tissue, it is challenging for a single material to have all three. Promising materials such as bioactive glass [2, 3], pulverized pig intestine [4, 5], interfacially engineered topographies [1], and growth factor–loaded autologous mesenchymal stem cell containing 3D printed grafts [6, 7] exist; however, bottlenecks that remain either due to their mechanism of action have not yet fully been revealed or they are too expensive or immunogenic [8]. A viable option is a simple, cheap, biocompatible, and inherently bioactive material interface that could potentially lead to an improvement in osteoconduction, osteoinduction, and osteogenesis.

The employment of silk as a tissue engineering scaffold material dates back to times before the invention of tissue engineering as a field. Silk is produced by members of the Lepidoptera family but more so by domesticated silkworm

✉ Tugba Ozdemir
tugba.ozdemir@sdsmt.edu

[1] Department of Medical Services and Techniques, Tokat Gaziosmanpasa University, Tokat, Turkey

[2] Department of Metallurgical Engineering, Sivas Cumhuriyet University, Sivas, Turkey

[3] Material Science and Engineering, University of Illinois Urbana-Champaign, Urbana, IL, USA

[4] Department of Pharmaceutical Biotechnology, Faculty of Pharmacy, Tokat Gaziosmanpasa University, Tokat, Turkey

[5] Department of Nanoscience and Biomedical Engineering, South Dakota School of Mines and Technology, Rapid City, SD, USA

Bombyx mori. The silk fiber forming the cocoon consists of two proteins namely fibroin and sericin [9]. Fibroin is the load-bearing component of the fiber, while sericin is thought to be a protective glue molecule keeping the cocoon hydrated and protected from UV rays [10]. Earlier studies of silk membrane implantation without removing sericin led to immune reactions which convinced the silk community to consider sericin as an unwanted component of tissue regeneration [11]. Sericin is a hydrophilic globular protein primarily adopting an amorphous random coil secondary structure and consists of 18 amino acids with much abundance of serine (33.4%), aspartic acid (16.7%), and glycine (13.5%) [11, 12]. Sericin has been successfully utilized in skin regeneration [13], cancer reversal strategy [14], and bone tissue engineering for both the normal [15–21] and diseased bone tissue [22]. In addition, sericin is also utilized as an implant coating to improve the bone-implant interface [16, 23, 24]. Despite growing numbers of evidence supporting the suitability of sericin as bone regenerative material, sericin is mechanically unfit, and its processibility and water solubility possess difficulties in utilizing sericin as a scaffold base component [11].

Hydroxyapatite (HAp) is a mineral consisting primarily of calcium phosphate and constitutes the inorganic part of bone tissue. HAp contributes to the compressive strength of bone tissue and is successfully used as a cement in bone tissue engineering scaffolds. Different methods have been utilized to form HAp crystals in biomaterials. One of the facile methods to form HAp crystals is the calcination of pulverized bones [25]. The addition of HAp into sericin as a bone filler was employed and reported to improve the mechanical performance of the resulting bone [26, 27]. On the other hand, sericin-HAp (Ser-HAp) scaffolds lack ductility as being a ceramic (an inorganic) material does not allow it to be used more than filler powders unless they were pelletized and sintered.

Electrospinning is a simple yet versatile technique to produce nanoparticles, nanofibers, nanoribbons, and core-shell nanostructures [28]. In particular, interconnected fibrillar materials produced by electrospinning are reminiscent of the extracellular matrix (ECM) [29]. Through driving electrocharged polymers onto a grounded conductive collector not only polymeric biomaterials but also inorganic molecules, proteins, and carbohydrates bioactive small molecules can be formed into highly porous, fibrillar, and interconnected meshes [28, 30]. The electrospun matrices provide the topography [31], architecture [30], and structure [32] needed to contain cells while differentiating into desired cell types. In addition, nanofibrous structures reminiscent of bone-like ECM have shown to activate a multitude of signaling pathways associated with the regeneration [33] thus proving inherent osteoinduction capacity.

In this study, we aimed to fabricate a bone regenerative scaffold that could provide osteoconductive, osteoinductive, and osteogenic components at the same time. Using Ser-HAp as the base material, we formed electrospun nanoribbons through a carrier polymer poly(vinyl alcohol) (PVA). The resultant nanoribbons were characterized using scanning electron microscopy (SEM), Fourier transform infrared spectroscopy (FTIR), and energy-dispersive spectroscopy (EDS) to assess the resulting material properties. SaOS-2 cells were cultured on sericin and Ser-HAp nanoribbons. The cellular adhesion, proliferation, and cytoskeletal organization were assessed for all surface types. Furthermore, in vitro, mineralization was quantified using a modified Alizarin Red staining method to reveal the contribution of each scaffold component in mineralization density. We hypothesized that combining Ser-HAp as a base material will lead to an enhanced osteoblast response toward mineralization.

Materials and methods

Materials

Bombyx mori silkworm cocoons were purchased from Kozabirlik Company (Bursa, Turkey). Poly(vinyl alcohol) (PVA) (205,000 Da) was purchased from Fluka (Buchs, Switzerland). Glutaraldehyde (50%), ethyl alcohol, and hydrochloric acid (HCl) were purchased from Thermo Fisher Scientific (Tewksbury, USA). McCoy's 5A cell culture medium was obtained from ATCC (Manassas, VA, USA). Fetal bovine serum (FBS), penicillin/atreptomycin (Penn/Strep), and trypsin/EDTA (0.25%) were purchased from Thermo Fisher Scientific (Carlsbad, CA, USA).

Sericin extraction

Silk sericin protein was extracted, purified, and dried in the laboratory using *Bombyx mori* silkworm cocoon through the direct boiling method to avoid salts in the final product following previously published methods [14]. Briefly, cocoons were first cleaned and minced into small pieces. Five grams of cleaned silkworm cocoons was weighed and autoclaved in 200 mL distilled water at 120 °C for 60 min. The silk solution was allowed to cool before being filtered through a 0.2-μm filter. The filtrate dried under vacuum until a fully dried brittle membrane was achieved. The membrane was then transferred to a mortar and pestle to grind rigorously to achieve sericin powder.

Production of nano-hydroxyapatite powders (n-HAp)

Hydroxyapatite powders from bovine bones were prepared earlier [25]. Briefly, freshly collected bone femoral parts

were cleaned, boiled in distilled water thrice, and decreased by 70% EtOH. The cleaned bone pieces were kept in NaClO (30% v/v) for at least 48 h and allowed to dry for further processing. Dried bone pieces were calcined at 1000 °C with a heating rate of 5 °C min^{-1} and kept at that temperature for 2 h in the air, as described elsewhere [1, 25]. Calcined bovine femoral bone parts were crushed in a mortar and pestle and then put in 250-mL HDPE (high-density polyethylene) jars at 300 rpm for 144 h with a 5:1 ball-to-powder ratio in a ball mill to reduce the particle size down to 100 nm.

Scaffold fabrication

A blend solution of sericin at 6% w/v and PVA at 10% w/v with or without 1% w/v of HAp in distilled water as solvent was transferred to a 5-mL syringe with a 21 G needle and loaded onto a syringe pump which is set to 0.4 mL/h. After a droplet of polymer solution is observed at the tip of the needle, the voltage is set to 13 kV with a needle-to-collector distance of 20 cm. Glass coverslips were attached to the conductive collector with a double-sided tape and allowed to collect nanoribbons for 10 min until a thick layer of the translucent membrane was developed.

Field emission scanning electron microscopy (FE-SEM) and energy-dispersive spectroscopy (EDS) analysis

The microstructure of the scaffolds and n-HAp powder was observed by field emission scanning electron microscope (FE-SEM, TESCAN Mira3 XMU, Czechia) under 15 kV accelerating voltage and 15 cm working distance, and transmission electron microscope (TEM) module was mounted onto SEM stage to obtain STEM on FE-SEM. The operating voltage was 30 kV, and the working distance was adjusted to 3 mm to evaluate the sample on the Cu grid more accurately. Composition analysis was performed using energy-dispersive spectroscopy apparatus attached to a scanning electron microscope with an analytical distance of 10 mm on SEM (EDS, INCA IE 350, and UK).

FTIR study of the surface

The surface chemical signatures of the different scaffolds were assessed with FTIR spectroscopy using Jasco 2000 Spectra (Tokyo, Japan). Using the ATR function, the fiber chemical bond vibrations were characterized using infrared light and tabulated using the Spectra Viewer software.

Scaffold conditioning

The coverslips coated with four different nanoribbons were placed in 6-well plates. Firstly, the plates were exposed to UV light for 45 min, and then, ethanol solution (70%) was added to each well and incubated at room temperature for 45 min. After that, the ethanol solution was removed from each well and then waited for a while for evaporation of the residue ethanol. McCoy's 5A (modified) medium containing 10% fetal bovine serum, 1% penicillin, 3 mM β-glycerophosphate, and 10 µg/mL ascorbic acid was added to each well to provide nanoribbons media conditioning. All plates were incubated overnight in a humidified atmosphere of 5% CO_2 at 37 °C.

Cell culture

A human osteogenic sarcoma cell line (SaOS-2) was used in this study (purchased from the cell bank of Turkey Foot and Mouth Disease Institute (HÜKÜK)). The initial cell concentration was adjusted to 1×10^6 cell/ mL, 50 µL of this cell suspension was seeded to cover the nanoribbon-coated coverslips in each well, and then, the plates were incubated in a humidified atmosphere of 5% CO_2 at 37 °C for 1 h. After that, each well was completed with sufficient medium, all plates were kept in a humidified atmosphere of 5% CO_2 at 37 °C, and the media was replaced three times per week until the end of the study.

Fixation

A fixation protocol was applied for all the samples. First, the samples taken on the 1st, 7th, and 14th days were placed in a new 6-well plate, each well was washed with 2.0 mL of $1\times$PBS (phosphate-buffered saline) solution, and then, 2.5 mL paraformaldehyde (PFA) was added to each well after waited at room temperature for 15 min. After that, the PFA was removed from each well, and each well was washed three times with $1\times$ PBS solution. For the adherent cells on nanoribbons stabilization, PB (permeabilization buffer) containing $1\times$ PBS, 2% BSA (bovine serum albumin), and 0.1% Triton X-100 was used, 2.5 mL PB was added to each well, and the edges of the plates were wrapped with parafilm to storage at +4 °C.

Alizarin Red S staining quantification assay

Alizarin Red S (ARS) staining method was modified to evaluate calcium deposits in adherent cells on the coverslips coated with different nanoribbons [34]. The coverslips coated with nanoribbons were cultured with SaOS-2 cell line and incubated in a humidified atmosphere of 5% CO_2 at 37 °C for 14 days, and then, the fixation protocol was applied to each of the samples. After removing the fixative, the samples were washed three times with distilled water. Following this, the distilled water was removed completely, and 1 mL of 40 mM ARS (pH= 4.2) was added to each well and incubated at room temperature for 30 min with gentle shaking. After aspirating dye from the wells, each well was washed five times

with distilled water. The stained nanoribbons were visualized by a phase contrast microscope, and the images were saved.

For quantification of staining, 800 μL of prepared 10% acetic acid solution was added to each well including coverslips of 6-well plates and incubated at room temperature for 30 min with shaking, and then, the cells were collected using a cell scraper and transferred to a 1.5-mL microcentrifuge tube. After each microcentrifuge tube was mixed for 30 s by using a vortex device, the tubes were heated at 85 °C for 10 min. Before heating, the tubes were sealed with parafilm to avoid evaporation. The tubes were then left in an ice bath for 5 min, the tubes were centrifuged at 20.000 g for 15 min, and then, 500 μL of supernatant was transferred to a new tube. Two hundred microliters of previously prepared 10% ammonium hydroxide was added to each tube for neutralization. One hundred fifty microliters of the sample was taken from each tube and transferred to 96-well plates, and the absorbance was read at 405 nm using a plate reader.

To calculate the ARS concentration in the samples, 4 mM ARS standard solution was prepared in a 1.5-mL microcentrifuge tube. After adding 500 μL of distilled water was added to each microcentrifuge tube, standart solutions were obtained in the concentration range of 2 mM ARS - 0.0313 mM ARS by serial dilution method. After the standart ARS solutions were prepared, 150 μL of each concentration was transferred to triplicate wells of 96 well plates, and the absorbance was read at 405 nm. The standard curve was drawn as concentration versus absorbance. After the trend line and equation were determined, ARS concentration in the samples was calculated depending on the equation and the trend line.

Immunofluorescence staining

After the fixation protocol was applied to the scaffolds taken on days 1, 7, and 14, the scaffolds were stained with DAPI (4′,6-diamidino-2-phenylindole) and phalloidin stain to evaluate cell proliferation and cell differentiation [35]. While the phalloidin is used to localize the F-actin, DAPI labels the nucleus. Firstly, the scaffolds were stained with phalloidin for 30 min in a dark place followed by washing three times with 1× PBS, and nuclei were labeled with DAPI for 5 min. The mounting media was not used because the DAPI was in the mounting media. The cells were imaged by fluorescence microscopy, and the total cell number and cell areas were determined by NIH ImageJ software.

Statistical analysis

The statistical differences between scaffolds were tested using a 2-sample Student's t-test. Samples with $p<0.05$ were accepted as statistically significant. When more than two groups were compared, one-way ANOVA with Tukey's test was performed to identify statistical significance. All biological experiments were done with a sample size of 3.

Results

Preparation and characterization of the nano-hydroxyapatite powders

Nano-hydroxyapatite (n-HAp) powder was prepared and characterized for uniformity before addition to the scaffolds (Fig. 1A, B). Before FE-SEM imaging, the sericin and Ser-HAp scaffolds were gold sputtered and investigated. The powders were then ball milled, and
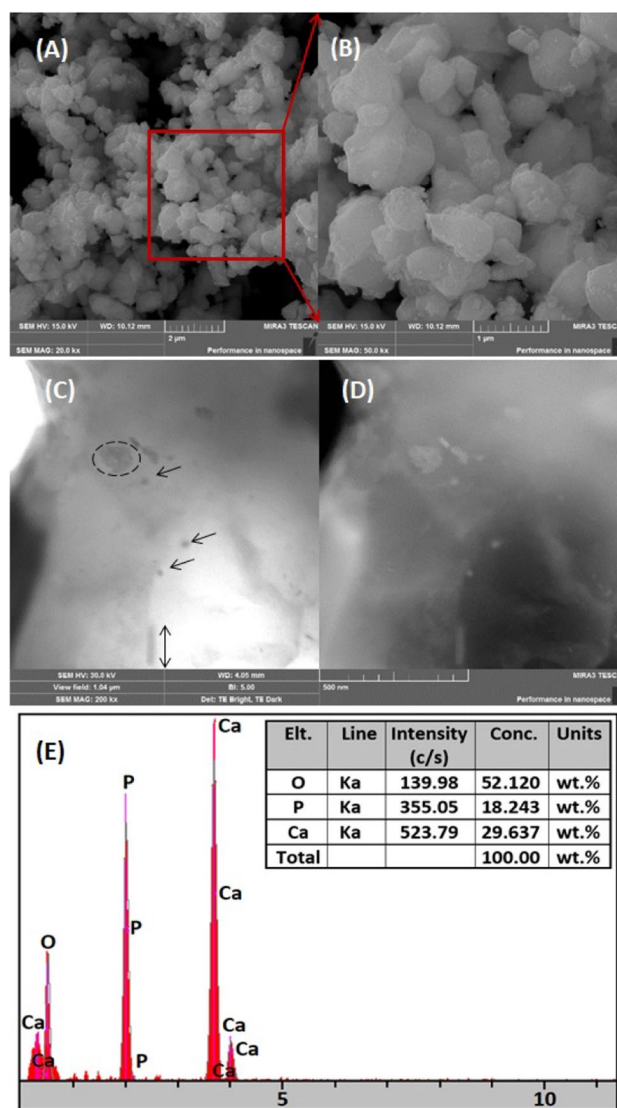

Fig. 1 Characterization of the hydroxyapatite (HAp) powders produced after the calcination process. **A**, **B** SEM images of the HAp powders at ×20,000 and ×50,000 magnifications. **C**, **D** n-HAp powders after ball milling for 144 h in S-TEM at 200 Kx magnifications, bright field (**C**) and dark field imaging (**D**), **E** the energy dispersive spectrometry and table representing the chemical composition of the produced n-HAp powders

nanopowders of lower than 100 nm particle size were achieved after 144 h of grinding. The n-HAp powders were measured to have 37.01 ± 11.37 nm diameter by S-TEM as shown in Fig. 1C, D. As it was evident from S-TEM images under bright field imaging mode, n-HAp particles were seen as fine aggregates about 30–40 nm diameter being mostly spherical (as shown by a dashed ellipse), and needle- and flake-like (as shown by double side arrow and short arrows) particles were found. By investigating under the S-TEM dark-field imaging mode, the coarser particles were also seen at about 200 nm both being needle and spheroid in shape nucleated and grown from finer seeds, especially that needle-shaped HAp powders intend to grow in the c direction due to the hexagonal lattice of HAp. EDS results indicate that the particulate matter is composed of 50.12% w/w oxygen (O), 18.24 % w/w phosphorus (P), and 29.63 % w/w calcium (Ca) with a corresponding spectrum which would be mostly a hydroxyapatite compound with a formula of $Ca_{10}(PO_4)_6(OH)_2$ (Fig. 1E) where Ca/P ratio is about 1.625, as being close to 1.66 as of in the above formula. By the addition of HAp, the coating of HAp by sericin could be attributed to the similar charge of HAp with PVA to be colloidally suspended in solution and remains parallel to deposition onto the collector side.

While being deposited onto the collector, PVA also covers HAp to maintain the prospective ribbon formation as was also evident from Fig. 2B, shown by arrows. Sericin as shown in Fig. 2A was found to have a decent structure of fibrils where Ser-HAp scaffolds have been seen as similar fibrils that makes them good and promising candidates for open wounds in the mouth environment to be bone forming and vascularization developers. Figure 2C is the EDS spectrum of elements for Fig. 2B (i) as seen by white arrows, and Ca, P, and O species along with C, due to fibrils, are evident.

Morphological and chemical characterization of nanoribbons

The electrospun matrices show interconnected and fibrillar morphology. The nanoribbons from sericin (Fig. 2A) and Ser-HAp (Fig. 2B) showed that there were no significant morphological differences between the nanoribbons. The fibrillar portion of the nanoribbons was measured and sericin nanoribbons were found to have 98.71 ± 23.03 nm, and Ser-HAp fibrils were found to have 81.77 ± 14.18 nm. The difference in diameter of the fibrils between groups was not statistically significant. The produced scaffolds were also analyzed for their chemical signatures. The sericin nanoribbons (Fig. 3, green) show an OH^- stretch at 3250 cm^{-1} indicating the presence of PVA and peak at 1250 cm^{-1}, 1500 cm^{-1}, and 1750 cm^{-1} indicating amide III, II, and I bond respectively. The addition of HAp resulted in PO_4^{-3} asymmetric bending vibration at 571 cm^{-1} and PO_4^{-3} asymmetric stretching at 1041 cm^{-1} shown in sericin-HAp (Fig. 3, blue) [36].

Fig. 2 SEM morphological characterization of the sericin and sericin-HAp nanoribbons after electrospinning: **A** the sericin nanoribbons at 20 Kx magnification and **B** sericin-HAp nanoribbons at 20 Kx magnification. **C** EDS analysis was done on the particulate matter embedded on the fibers shown by white arrows (**B**, (i)) to confirm chemical composition (**C**, (ii))
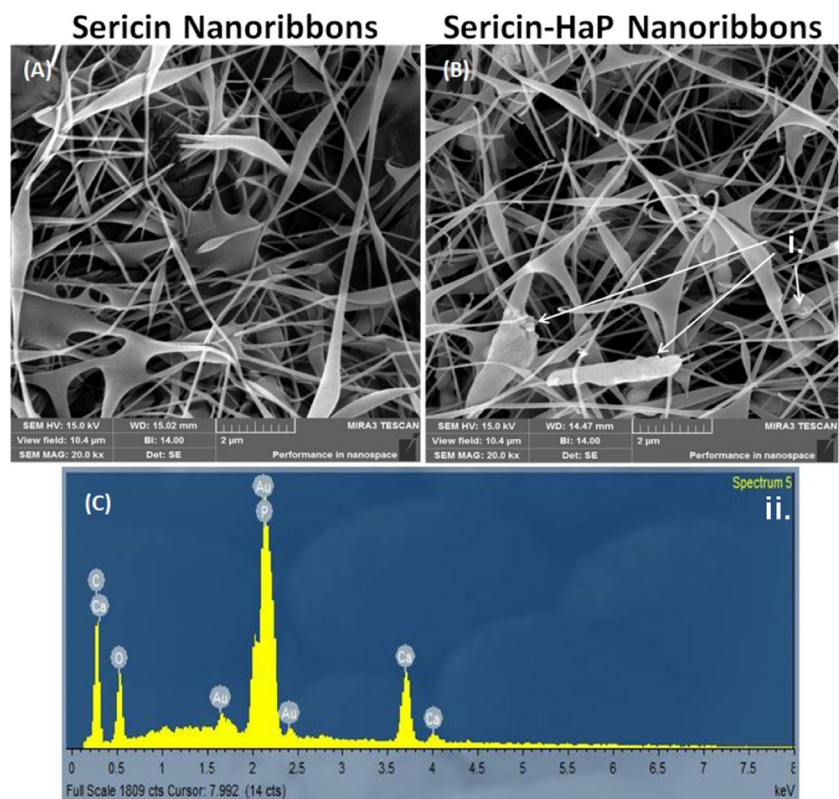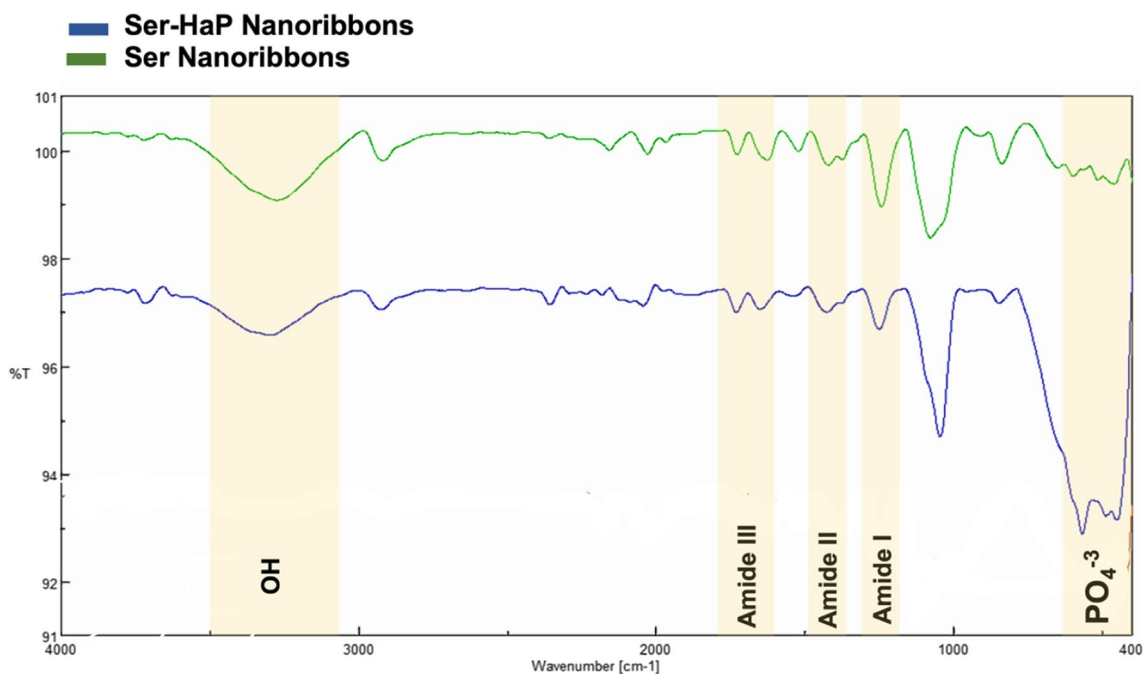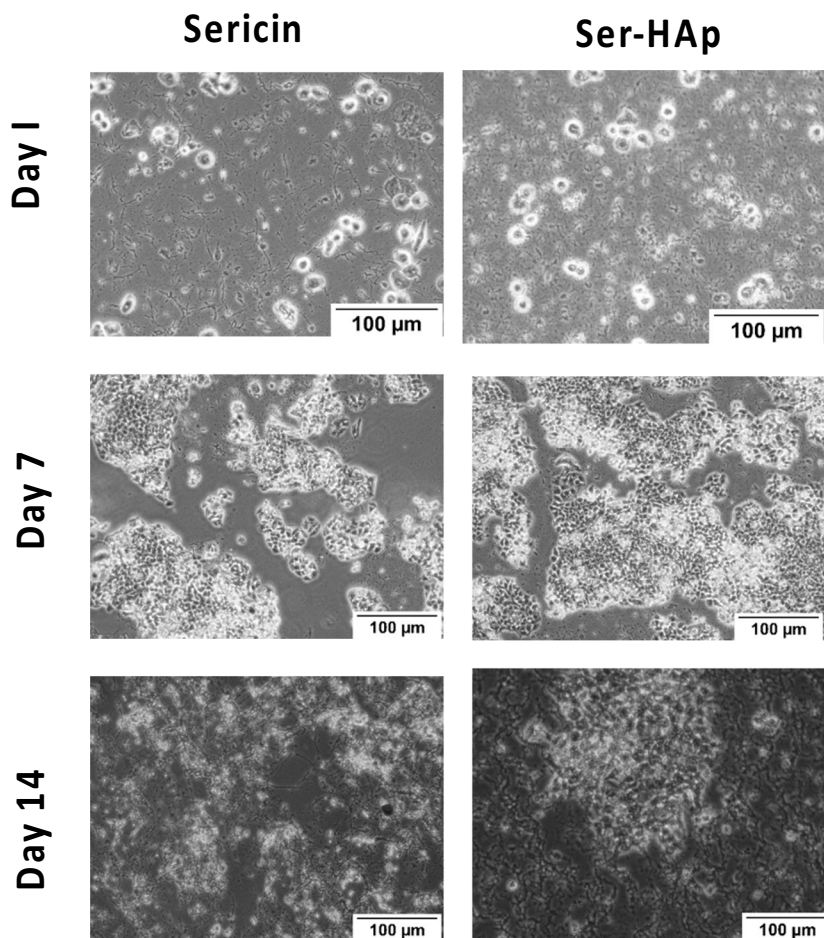
Fig. 3 FTIR spectra of the sericin (green) and Ser-HAp (blue) nanoribbon scaffolds

Fig. 4 Brightfield microscopy images of the SaOS-2 cells cultured on sericin and Ser-HAp nanoribbons deposited on glass coverslips on Day 1, Day 7, and Day 14. Images were taken at 10x magnification (n=5).
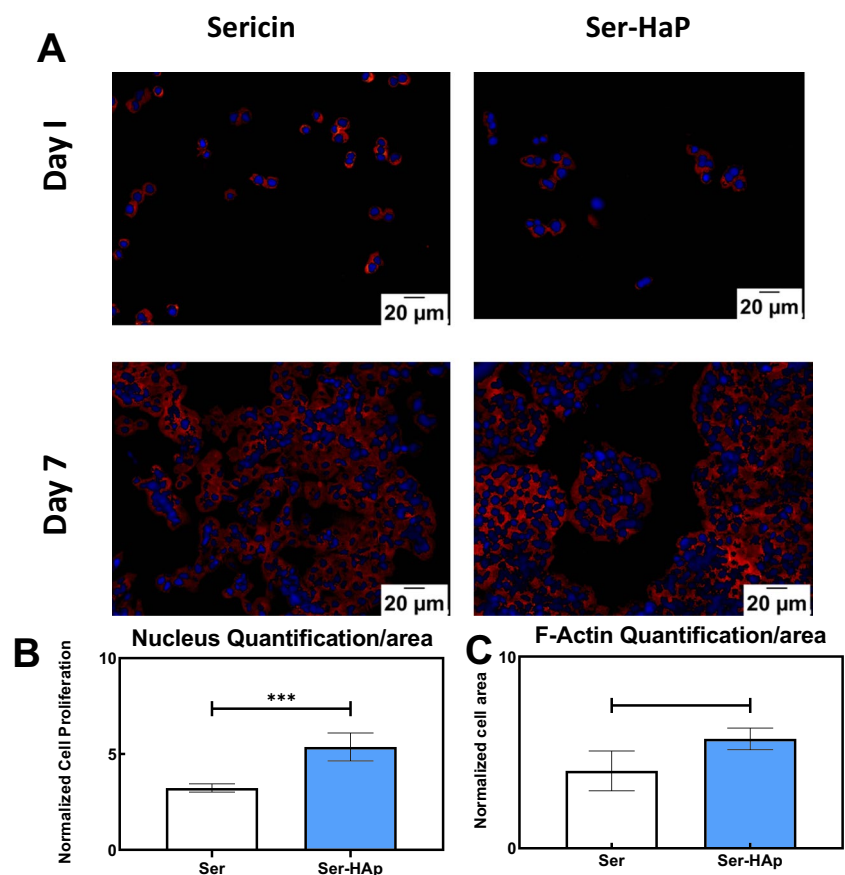
Osteoblast cell morphology and scaffold coverage

The bright field images on scaffold-coated glass coverslips were monitored for 14 days. Cells appear to cover the scaffold deposited surfaces as early as 7 days for both sericin and Ser-HAp surfaces. Based on cell coverage and overall morphology, all scaffolds were observed to support cell adhesion and coverage (Fig. 4).

Osteoblast cell proliferation and adhesion on scaffolds

Osteoblasts were fixed and immunostained for F-actin and nucleus on day 1 and day 7 respectively (Fig. 5A). Cell proliferation was monitored using nuclear signal quantification on day 7/day 1 and normalized to the surface area for each group. DAPI signal increased 3.22-fold for sericin scaffolds, while it increased 5.37-fold for Ser-HAp scaffolds (Fig. 5B). The F-actin signal was measured on day 7/day 1 and normalized to the surface area. F-actin is a cytoskeletal element; its levels increase with increased surface adhesion. The F-actin signal increased 4.04-fold for sericin scaffolds, while the Ser-HAp scaffolds showed a 5.71-fold increase in the F-actin signal (Fig. 5C).

Assessment of osteoinduction through ARS

Newly formed mineralization could be monitored by staining with Alizarin Red dye. ARS appears as red under a bright-field microscope, and further analysis of ARS concentrations positively correlates with mineralization density. The gross morphology of cell monolayers on day 14 before and after ARS is shown in Fig. 6. The quantitative ARS concentration is shown in Fig. 6. The figure inset shows the ARS dye signal used as a standard for ARS signal quantification. As shown in Fig. 6, sericin scaffolds adsorb 0.1084 ± 0.0235 nM ARS, while Ser-HAp scaffolds adsorb 0.1388 ± 0.0308 nM respectively.

Discussion

Considering 70% of the bone is composed of inorganic content [37], it is critical to create a bone regenerative scaffold leading to high mineralization density. In this study, we fabricated a nanoribbon-like scaffold structure not only by combining sericin (an osteoinductive silk protein) and HAp (bone mineral) to provide higher surface area, porosity, and ECM mimetic architecture as opposed to coating [23, 24, 38]. Our results supported that Ser-HAp scaffolds possess

Fig. 5 **A** Fluorescence microscopy images of the SaOS-2 cells stained against F-actin (red) and nucleus (blue) on sericin and Ser-HAp nanoribbons deposited on glass coverslips on day 1 and day 7. Images were taken at ×20 magnification. **B** Quantification of the nuclear fluorescence signal at day 7 normalized to day 1 (n=9 images). **C** Quantification of the F-actin fluorescence signal at day 7 normalized to day 1 (n=9 images). Values are represented as mean±SD and *p<0.05, ***p < 0.001

Fig. 6 Brightfield microscopy images of the SaOS-2 cell Alizarin Red staining (ARS) against mineral deposition on sericin and Ser-HAp nanoribbons deposited on glass coverslips on day 14. Images were taken at ×20 magnification. Alizarin red concentration graph represents the average mineral concentration on day 14 (figure inset represents the ARS standard used to quantify the ARS signal). Values are represented as mean±SD
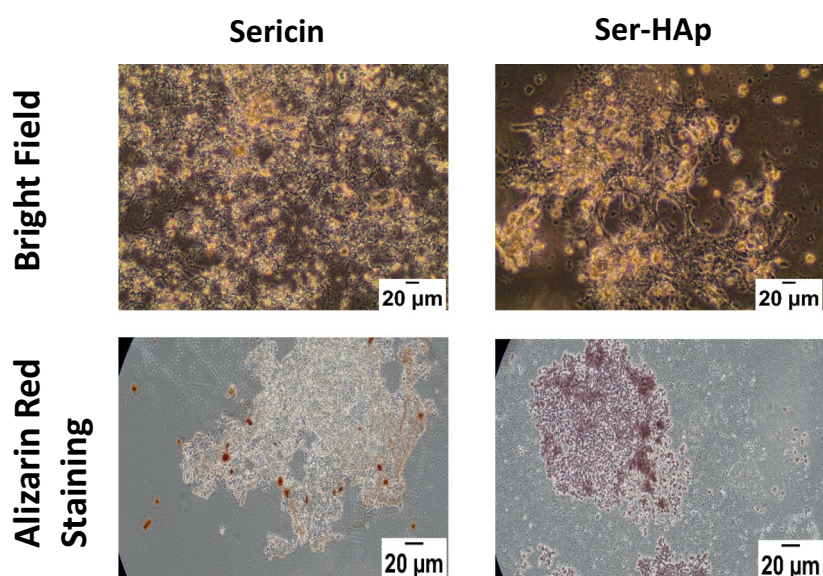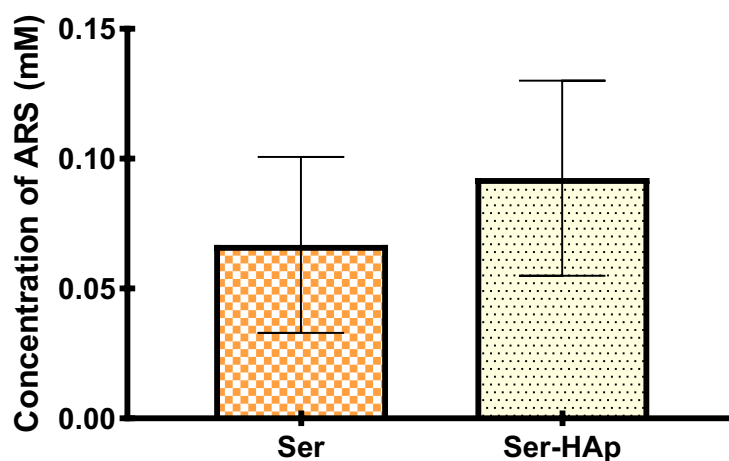
enhanced mineralization content compared to sericin-only nanoribbons. This provides a good insight into future works for in vitro or in vivo fracture formation and their fast repair by those material combinations.

We chose sericin as our base scaffold component due to its interesting properties in the bone regeneration [39]. Not until recently, sericin was considered an industrial byproduct of silk fiber production in the textile industry owing to its misunderstood complex immunogenicity [40]. Recently, it is discovered that MC3T3E1 osteoblasts in vitro and sericin-coated gelatin sponge implantation in a rat calvarial critical-size bone defect model in vivo [41, 42]. Our method of extracting sericin using hot water allowed our purpose to target mineral deposition in our scaffolds. As supported by our mineralization results, sericin-only scaffolds alone supported mineralization for 14

days after cell seeding. The immunogenicity and even osteogenic properties highly rely on the procedure by which sericin is extracted [43]. Concerning the immunogenicity of sericin, two main pieces of information are known so far. First, sericin extracts from boiled and filtered cocoons innately allow HAp nucleation on surfaces without forming crystals [44, 45]; second, high molecular weight (>30 kDa) sericin extracted by sonicating at 37 °C exhibits osteo-immunomodulation [46] through increased bone morphogenic protein 2/4 (BMP 2/4) via macrophage Toll-like receptor signaling in both coculture of Raw264.7 cells.

Initial promising results on sericin-coated surfaces exhibiting HAp nucleation reported that the resulting minerals, however, would not lead to biomimetic crystal formation. The hot water sericin extraction (which is considered to be

least toxic to cells [40]) led to an enhanced semi-crystalline β-sheet formation through alternating glutamic acid and aspartic acid side chain groups exposed, which were reported to be attracting ions and resulting in local supersaturation of the molecules, thus leading to mineralization [47, 48]. When examined closely, these minerals showed nanorod-like structures with low crystallinity but still have an orientation toward the *c*-axis exhibiting similarity with native hydroxyapatite [47]. It is also noteworthy that the HAp in sericin is intended to attract bone material to facilitate good bonding and faster mineralization in jaw bones and maxillofacial crane structures and can also be used as fillers, as described elsewhere [25]. To boost the mineralization observed with sericin, n-HAp powders were introduced together in microcapsule [27] or micro/nanoparticle forms as bone fillers [49, 50]. Therefore, introducing sericin along with HAp is reported to boost osteogenic response.

Topography and the radius of curvature provided by scaffolds are other important parameters that need to be clarified early in the scaffold design [1]. For instance, we showed fibrillar polymeric scaffolds presenting a 1.5 µm diameter increase in the early osteoinduction-associated mechanotransduction [33]. Our nanoribbons were aimed to provide high surface area and porosity rather than osteoinductive geometry for this study. Future investigations will work on optimizing the scaffold geometry along with the Ser-HAp content to achieve the highest cellular outcome. We also recognize the importance of the sericin extraction process and believe that using a homogenous sericin protein with high molecular weight will lead to immuno-osteogenicity as reported earlier.

We found when combined, Ser-HAp scaffolds lead to the highest mineralization content and proliferation. In addition, F-actin content was also significantly higher than in sericin-only scaffolds. These results together with the results obtained from Ser-HAp scaffolds indicate that sericin and HAp synergistically enhance mineralization on nanoribbon-shaped scaffolds. We propose that introducing Ser-HAp together is a promising strategy to be used as dental implant interfaces and accelerate the healing of short and narrow bone substitutes and bone fillers.

Conclusion

Osteoinductive Sericin is combined with HAp in electrospinning method to form scaffolds with an increased surface area that are highly porous and structurally reminiscent of bone extracellular matrix analogue. The produced scaffolds increased osteoblast cell proliferation and cytoskeletal organization significantly. Furthermore, the elevated mineral density on the composites supports the utility of the scaffolds for future applications. Future work will target cell adhesive

sequences (in vitro/in vivo) to promote further cellular adhesion on the nanoribbons with optimized nanofibrous topography and gain a mechanistic understanding of Ser-HAp osteoinductive scaffolds.

Declarations

References

1. Ozdemir, T., Higgins, A.M., Brown, J.L.: Osteoinductive biomaterial geometries for bone regenerative engineering. Curr. Pharm. Des. **19**(19), 3446–3455 (2013)
2. Öksüz, K.: Effect of composition and sintering temperature on the structure and properties of porous bioactive glass scaffolds. Chiang Mai J. Sci. **46**, 568–578 (2019)
3. Jones, J.R., Gentleman, E., Polak, J.: Bioactive glass scaffolds for bone regeneration. Elements. **3**(6), 393–399 (2007)
4. Sharma, D.: New technologies in regenerative medicine. Indian J. Genet. Mol. Res. **5**(1), 19 (2016)
5. Choi, Y., Cox, C., Lally, K., Li, Y.: The strategy and method in modulating finger regeneration. Regen. Med. **9**(2), 231–242 (2014)
6. Bisht, B., Hope, A., Mukherjee, A., Paul, M.K.: Advances in the fabrication of scaffold and 3D printing of biomimetic bone graft. Ann. Biomed. Eng. **49**(4), 1128–1150 (2021)
7. Ji, X., Yuan, X., Ma, L., Bi, B., Zhu, H., Lei, Z., Liu, W., Pu, H., Jiang, J., Jiang, X.: Mesenchymal stem cell-loaded thermosensitive hydroxypropyl chitin hydrogel combined with a three-dimensional-printed poly (ε-caprolactone)/nano-hydroxyapatite scaffold to repair bone defects via osteogenesis, angiogenesis and immunomodulation. Theranostics. **10**(2), 725 (2020)
8. Amini, A.R., Laurencin, C.T., Nukavarapu, S.P.: Bone tissue engineering: recent advances and challenges, Critical Reviews™. Biomed. Eng. **40**(5), 363–408 (2012)
9. Ebrahimi, D., Tokareva, O., Rim, N.G., Wong, J.Y., Kaplan, D.L., Buehler, M.J.: Silk-its mysteries, how it is made, and how it is used. ACS Biomater. Sci. Eng. **1**(10), 864–876 (2015)
10. Kwon, K.-J., Seok, H.: Silk protein-based membrane for guided bone regeneration. Appl. Sci. **8**(8), 1214 (2018)
11. Kunz, R.I., Brancalhão, R.M.C., de Fátima Chasko Ribeiro, L., Natali, M.R.M.: Silkworm sericin: properties and biomedical applications. Biomed. Res. Int. **2016**, 8175701 (2016)
12. Arango, M.C., Montoya, Y., Peresin, M.S., Bustamante, J., Álvarez-López, C.: Silk sericin as a biomaterial for tissue engineering: a review, International Journal of Polymeric Materials and Polymeric. Biomaterials. **70**(16), 1115–1129 (2021)
13. Qi, C., Xu, L., Deng, Y., Wang, G., Wang, Z., Wang, L.: Sericin hydrogels promote skin wound healing with effective regeneration of hair follicles and sebaceous glands after complete loss of epidermis and dermis. Biomater. Sci. **6**(11), 2859–2870 (2018)
14. Yan, S., Li, X., Dai, J., Wang, Y., Wang, B., Lu, Y., Shi, J., Huang, P., Gong, J., Yao, Y.: Electrospinning of PVA/sericin

nanofiber and the effect on epithelial-mesenchymal transition of A549 cells. Mater. Sci. Eng. C. **79**, 436–444 (2017)

15. Wang, F., Hou, K., Chen, W., Wang, Y., Wang, R., Tian, C., Xu, S., Ji, Y., Yang, Q., Zhao, P.: Transgenic PDGF-BB/sericin hydrogel supports for cell proliferation and osteogenic differentiation. Biomater. Sci. **8**(2), 657–672 (2020)

16. Voicu, S.I., Condruz, R.M., Mitran, V., Cimpean, A., Miculescu, F., Andronescu, C., Miculescu, M., Thakur, V.K.: Sericin covalent immobilization onto cellulose acetate membrane for biomedical applications. ACS Sustain. Chem. Eng. **4**(3), 1765–1774 (2016)

17. Vedakumari, S.W., Jayalakshmi, R., Sanjayan, C., Jayavardhini, B., Arya, K., Murugesan, R.: Fabrication of microcomposites based on silk sericin and monetite for bone tissue engineering. Polym. Bull. **77**(1), 475–481 (2020)

18. Pankongadisak, P., Suwantong, O.: The potential use of thermosensitive chitosan/silk sericin hydrogels loaded with longan seed extract for bone tissue engineering. RSC Adv. **8**(70), 40219–40231 (2018)

19. Pankongadisak, P., Jaikaew, N., Kiti, K., Chuenjitkuntaworn, B., Supaphol, P., Suwantong, O.: The potential use of gentamicin sulfate-loaded poly (l-lactic acid)-sericin hybrid scaffolds for bone tissue engineering. Polym. Bull. **76**(6), 2867–2885 (2019)

20. Kweon, H., Jo, Y.-Y., Seok, H., Kim, S.-G., Chae, W.-S., Sapru, S., Kundu, S.C., Kim, D.-W., Park, N.-R., Che, X.: In vivo bone regeneration ability of different layers of natural silk cocoon processed using an eco-friendly method. Macromol. Res. **25**(8), 806–816 (2017)

21. Jiang, L.-B., Ding, S.-L., Ding, W., Su, D.-H., Zhang, F.-X., Zhang, T.-W., Yin, X.-F., Xiao, L., Li, Y.-L., Yuan, F.-L.: Injectable sericin based nanocomposite hydrogel for multi-modal imaging-guided immunomodulatory bone regeneration. Chem. Eng. J. **418**, 129323 (2021)

22. Noosak, C., Jantorn, P., Meesane, J., Voravuthikunchai, S., Saeloh, D.: Dual-functional bioactive silk sericin for osteoblast responses and osteomyelitis treatment. PLoS One. **17**(3), e0264795 (2022)

23. Marvi, M.S., Nourmohammadi, J., Ataie, M., Negahdari, B., Naderi, M.: Surface modification of titanium implants via electrospinning of sericin and Equisetum arvense enhances the osteogenic differentiation of stem cells. Int. J. Polym. Mater. Polym. Biomater. **71**(13), 1–12 (2021)

24. Karaji, Z.G., Jahanmard, F., Mirzaei, A., Van der Wal, B., Yavari, S.A.: A multifunctional silk coating on additively manufactured porous titanium to prevent implant-associated infection and stimulate bone regeneration. Biomed. Mater. **15**(6), 065016 (2020)

25. Öksüz, K.E., Kilinç, S., Özer, A.: Effect of calcination on microstructure development and properties of hydroxyapatite powders extracted from human and bovine bones. Trans. Indian Ceram. Soc. **78**(1), 41–45 (2019)

26. Veiga, A., Castro, F., Rocha, F., Oliveira, A.L.: Recent advances in silk sericin/calcium phosphate biomaterials. Front. Mater. **24**, 1–14 (2020)

27. Li, W., Cai, Y., Zhong, Q., Yang, Y., Kundu, S.C., Yao, J.: Silk sericin microcapsules with hydroxyapatite shells: protection and modification of organic microcapsules by biomimetic mineralization. J. Mater. Chem. B. **4**(2), 340–347 (2016)

28. Ramakrishna, S., Fujihara, K., Teo, W.-E., Yong, T., Ma, Z., Ramaseshan, R.: Electrospun nanofibers: solving global issues. Mater. Today. **9**(3), 40–50 (2006)

29. Liu, Z., Ramakrishna, S., Liu, X.: Electrospinning and emerging healthcare and medicine possibilities. APL Bioeng. **4**(3), 030901 (2020)

30. Ramaseshan, R., Sundarrajan, S., Jose, R., Ramakrishna, S.: Nanostructured ceramics by electrospinning. J. Appl. Phys. **102**(11), 7 (2007)

31. Ozdemir, T., Xu, L.C., Siedlecki, C., Brown, J.L.: Substrate curvature sensing through myosin IIa upregulates early osteogenesis. Integr. Biol. (Camb.). **5**(11), 1407–1416 (2013)

32. Takeuchi, A., Ohtsuki, C., Miyazaki, T., Tanaka, H., Yamazaki, M., Tanihara, M.: Deposition of bone-like apatite on silk fiber in a solution that mimics extracellular fluid. J. Biomed. Mater. Res. Part A. **65**(2), 283–289 (2003)

33. Ozdemir, T., Bowers, D.T., Zhan, X., Ghosh, D., Brown, J.L.: Identification of key signaling pathways orchestrating substrate topography directed osteogenic differentiation through high-throughput siRNA Screening. Sci. Rep. **9**(1), 1001 (2019)

34. Gregory, C.A., Gunn, W.G., Peister, A., Prockop, D.J.: An Alizarin Red-based assay of mineralization by adherent cells in culture: comparison with cetylpyridinium chloride extraction. Anal. Biochem. **329**(1), 77–84 (2004)

35. Guerra, F.S., Oliveira, R.G., Fraga, C.A.M., Mermelstein, C.D.S., Fernandes, P.D.: ROCK inhibition with Fasudil induces beta-catenin nuclear translocation and inhibits cell migration of MDA-MB 231 human breast cancer cells. Sci. Rep. **7**(1), 13723 (2017)

36. Ch, A., Sagadevan, S., Dakshnamoorthy, A.: Synthesis and characterization of nano-hydroxyapatite (n-HAP) using the wet chemical technique. Int. J. Phys. Sci. **8**(32), 1639–1645 (2013)

37. Schwartz, Z., Kieswetter, K., Dean, D., Boyan, B.: Underlying mechanisms at the bone-surface interface during regeneration. J. Periodontal Res. **32**(1), 166–171 (1997)

38. Iranpour, S., Attari, F., Seyedjafari, E., Nourmohammadi, J.: Coating of 3D-printed poly (ε-caprolactone) scaffolds with silk protein sericin enhances the osteogenic differentiation of human mesenchymal stem cells. Polym. Adv. Technol. **33**(4), 1211–1221 (2022)

39. Wang, Z., Zhang, Y., Zhang, J., Huang, L., Liu, J., Li, Y., Zhang, G., Kundu, S.C., Wang, L.: Exploring natural silk protein sericin for regenerative medicine: an injectable, photoluminescent, cell-adhesive 3D hydrogel. Sci. Rep. **4**(1), 1–11 (2014)

40. Aramwit, P.: Bio-response to silk sericin, silk biomaterials for tissue engineering and regenerative medicine, pp. 299–329. Elsevier (2014)

41. Nayak, S., Dey, T., Naskar, D., Kundu, S.C.: The promotion of osseointegration of titanium surfaces by coating with silk protein sericin. Biomaterials. **34**(12), 2855–2864 (2013)

42. Jo, Y.Y., Kweon, H., Kim, D.W., Baek, K., Chae, W.S., Kang, Y.J., Oh, J.H., Kim, S.G., Garagiola, U.: Silk sericin application increases bone morphogenic protein-2/4 expression via a toll-like receptor-mediated pathway. Int. J. Biol. Macromol. **190**, 607–617 (2021)

43. Yang, M., Shuai, Y., Zhou, G., Mandal, N., Zhu, L., Mao, C.: Tuning molecular weights of Bombyx mori (B. mori) silk sericin to modify its assembly structures and materials formation. ACS Appl. Mater. Interfaces. **6**(16), 13782–13789 (2014)

44. Yang, M., Shuai, Y., Zhang, C., Chen, Y., Zhu, L., Mao, C., OuYang, H.: Biomimetic nucleation of hydroxyapatite crystals mediated by Antheraea pernyi silk sericin promotes osteogenic differentiation of human bone marrow derived mesenchymal stem cells. Biomacromolecules. **15**(4), 1185–1193 (2014)

45. Yang, M., Zhou, G., Shuai, Y., Wang, J., Zhu, L., Mao, C.: Ca 2+-induced self-assembly of Bombyx mori silk sericin into a nanofibrous network-like protein matrix for directing controlled nucleation of hydroxylapatite nano-needles. J. Mater. Chem. B. **3**(12), 2455–2462 (2015)

46. Jo, Y.-Y., Kweon, H., Kim, D.-W., Baek, K., Kim, M.-K., Kim, S.-G., Chae, W.-S., Choi, J.-Y., Rotaru, H.: Bone regeneration is associated with the concentration of tumour necrosis factor-α induced by sericin released from a silk mat. Sci. Rep. **7**(1), 1–12 (2017)

47. Takeuchi, A., Ohtsuki, C., Miyazaki, T., Kamitakahara, M., Ogata, S.-I., Yamazaki, M., Furutani, Y., Kinoshita, H., Tanihara, M.: Heterogeneous nucleation of hydroxyapatite on protein: structural effect of silk sericin. J. R. Soc. Interface. **2**(4), 373–378 (2005)

48. Tavafoghi, M., Cerruti, M.: The role of amino acids in hydroxyapatite mineralization. J. R. Soc. Interface. **13**(123), 20160462 (2016)

49. Veiga, A., Castro, F., Reis, C.C., Sousa, A., Oliveira, A.L., Rocha, F.: Hydroxyapatite/sericin composites: a simple synthesis route under near-physiological conditions of temperature and pH and preliminary study of the effect of sericin on the biomineralization process. Mater. Sci. Eng. C. **108**, 110400 (2020)

50. Das, G., Shin, H.-S., Campos, E.V.R., Fraceto, L.F., del Pilar Rodriguez-Torres, M., Mariano, K.C.F., de Araujo, D.R., Fernández-Luqueño, F., Grillo, R., Patra, J.K.: Sericin based nanoformulations: a comprehensive review on molecular mechanisms of interaction with organisms to biological applications. J. Nanobiotechnol. **19**(1), 1–22 (2021)